Optically tunable Quincke rotation of a nanometer-thin oblate spheroid

Yu Gu and Haibo Zeng*

MIIT Key Laboratory of Advanced Display Materials and Devices, Institute of Optoelectronics and Nanomaterials, College of Materials Science and Engineering, Nanjing University of Science and Technology, Nanjing 210094, China

(Received 13 June 2017; published 24 August 2017)

Ever since the discovery of Quincke rotation (spontaneous rotation of a particle in fluid under a dc electric field) more than 100 years ago [G. Quincke, Ann. Phys. (Leipzig) **295**, 417 (1896)], the strength of the dc field has been the only external parameter to actively tune the rotation speed. In this paper we theoretically propose an optically tunable Quincke rotor exploiting the photoconductivity of a semiconducting nanometer-thin oblate spheroid. A full analysis of the instability of the Quincke rotation reveals that, unlike a prolate spheroid, no bistability is possible in such a dynamical system. In addition, the required material property and the strength of the dc electric field needed to realize the rotation are also elucidated. It is also predicted that light can be used to tune the spinning speed or simply turn on and off the Quincke rotation very effectively.

DOI: 10.1103/PhysRevFluids.2.083701

I. INTRODUCTION

Quincke rotation, the spontaneous rotation of a sphere suspended in fluid under a dc electric field, was first discovered by Quincke [1]. In most cases, a particle suspended in fluid gets polarized under a dc field and keeps its orientation after reaching a steady state. Quincke rotation only occurs when the steady nonspinning state becomes unstable so that tiny perturbation will be amplified and the particle eventually settles to a continuous spinning state. As been summarized by Jones [2,3], to realize Quincke rotation of a sphere, two conditions must be met: (i) The charge relaxation time τ_p of the sphere ($\tau_p = \varepsilon_p/\sigma_p$, where ε_p is the permittivity and σ_p the conductivity) has to be greater than that of the surrounding fluid $\tau_f = \varepsilon_f/\sigma_f$ ($\tau_p > \tau_f$) and (ii) the electric field E_0 must surpass a certain threshold value E_c. Such spinning of particles can induce an apparent decrease of viscosity of a colloidal suspension [4,5] or an increase of its electric conductivity [6,7]. This effect was also actively involved in other interesting applications such as droplet shape manipulation [8], transport of particles in liquid crystals [9], and hydrodynamic-interaction-induced self-organization of particles [10,11].

In Quincke rotation, the rotation speed Ω of a sphere is proportional to $[(E_0/E_c)^2-1]^{1/2}$ [2], where E_c is the critical field determined by the fluid viscosity as well as the electrical conductivity and permittivity of both the fluid and particle. Therefore, in a typical experiment, the external electric field E_0 becomes the only parameter to control the rotation speed given the fact that E_c does not change once the particle geometry and material's properties are defined. To provide additional tuning parameters, one must be able to somehow vary the electric property of either the particle or fluid actively. It is natural to think about semiconductors whose electric conductivity can be varied by several orders of magnitude with ultraviolet (UV), visible, or infrared (IR) light [12]. Typical materials include ZnO, GaN, diamond, etc., for UV light; Si, CdS, $CsPbX_3$ (where X denotes Cl, Br, or I) perovskite, etc., for visible light; and Ge, InGaAs, PbS, etc., for IR light. Following this idea, one can design an optically tunable semiconducting Quincke rotor as schematically shown in Figs. 1(a) and 1(b). A micron-sized and nanometer-thin disklike particle is ideal for such applications as it allows uniform light absorption throughout the particle when its thickness is much smaller than

*Author to whom correspondence should be addressed: zeng.haibo@njust.edu.cn

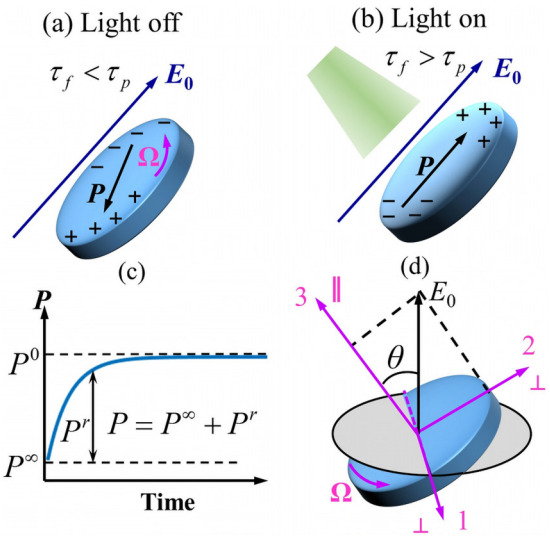

FIG. 1. (a) and (b) Turning off the Quincke rotation with light. When light is on, the conductivity of the disklike particle increases, so the condition $\tau_f < \tau_p$ is not satisfied anymore and the Quincke rotation becomes impossible. (c) Schematic showing the total polarization P, the high-frequency polarization P^∞, the retardation polarization P^r, and the equilibrium polarization P^0. (d) Definitions of angles and axes.

the light wavelength. For a microsphere or microsized prolate spheroid, Mie scattering results in nonuniform light intensity inside the particle causing diffusive current of the photogenerated charge carriers, which would significantly complicate the problem and make the rotation less controllable. However, to experimentally realize the optically tunable Quincke rotation for a thin oblate spheroid, one has to have a full understanding of the instability of the rotation regarding the material property and the external electric field. Surprisingly, although Quincke rotations of sphere and prolate spheroids have been well studied both theoretically and experimentally [2,3,13–15], there has been a very limited amount of work about disklike particles [16,17]. A detailed analysis on the instability of Quincke rotation of disklike particles is still missing even though the theoretical framework has already been set up in the work of Cēbers *et al.* [14].

In this paper we provide a theoretical analysis focusing on the instability and the optical tunability of Quincke rotation for thin nanoplates based on the dynamic model proposed by Cēbers *et al.* [14]. We present a detailed phase diagram illustrating the material selection as well as the electric field required for realizing Quincke rotation for a nanometer-thin oblate spheroid. The result indicates that the disk surface is always parallel to the electric field in both spinning and nonspinning states and no bistability will be observed. Meanwhile, it is predicted that light can be used to tune the spinning speed or simply turn on and off the Quincke rotation very effectively.

II. THEORETICAL MODEL

Taking the particle as the frame of the reference, Jones [2,3] treated the dc field as a rotating field with respect to the particle and introduced the complex permittivity $\varepsilon_i – i\sigma_i/\omega$ to explain the spontaneous rotation of a sphere. Briefly, the imaginary part results in a constant phase lag between the effective dipole moment of the particle and the rotating field that produces a constant torque sustaining the continuous rotation. From this perspective, this phase-locked rotation is similar to a magnetic particle rotating synchronously with a rotating magnetic field [18–21]. The complex permittivity model does not take into account the transient process prior to the steady state being achieved and falls short of a full analysis of the stability of the rotation. On the other hand, Cēbers [22]

presented a fully dynamic model considering a time-dependent effective dipole and later extended it to a prolate spheroid [14,23]. This model illustrated that to maintain a steady Quincke rotation, the convection current caused by the particle rotation is compensated by the conductive current so that the charge distribution on the particle surface (corresponding to the effective dipole) does not change with time and a constant torque can be maintained. The model was successfully applied to a prolate spheroid and the suggested bistability (Quincke rotation and steady orientation) has also been experimentally proved [13,14].

The dynamic model of Cēbers *et al.* is described as follows. Consider an ellipsoidal particle polarized under a dc electric field in a certain fluid. An effective dipole moment $\boldsymbol{p} = V\boldsymbol{P}$ (where V is the particle volume and $\boldsymbol{P}$ the effective polarization) is typically introduced to describe the force or torque exerted on the particle. Such an effective dipole comes from the so-called interfacial polarization that accounts for the formation of bounded charges at the interface due to the mismatch of permittivity between the particle and the fluid as well as the free-charge accumulation arising from their conductivity. The bounded charges are built almost instantaneously while the free charge is accumulated on the interface via the conduction current: the free-charge relaxation process. Therefore, one can divide the effective polarization $\boldsymbol{P}$ into a time-independent instantaneous polarization $\boldsymbol{P}^{\infty}$ accounting for the permittivity mismatch and a time-dependent retardation polarization $\boldsymbol{P}^{r}$ describing the charge relaxation process ($\boldsymbol{P} = \boldsymbol{P}^{\infty} + \boldsymbol{P}^{r}$) as illustrated in Fig. 1(c). The system reaches an equilibrium when the normal component of the conduction current is continuous at the particle surface. If one introduces the equilibrium polarization $\boldsymbol{P}^{0}$, i.e., polarization as time tends to infinity, and ignores any anisotropy for the moment, the relaxation of the polarization can be simply described as $\partial\boldsymbol{P}/\partial t = -(\boldsymbol{P}-\boldsymbol{P}^{0})/\tau$ or $\partial\boldsymbol{P}^{r}/\partial t = -(\boldsymbol{P}^{r} + \boldsymbol{P}^{\infty}-\boldsymbol{P}^{0})/\tau$ in terms of the retardation polarization (τ is the charge relaxation time). However, due to the shape anisotropy of a thin disk, one has to introduce a system of coordinates shown in Fig. 1(d) and decompose the polarization $\boldsymbol{P}$ along the three axes as P_1, P_2, and P_3. The system of coordinates is introduced in the following manner. Axis 3 is the axis of symmetry of the disklike particle forming an angle θ with the electric field E_0 and axis 1 is perpendicular to the plane formed by the electric field E_0 and axis 3. Axis 1 is also known as the line of nodes for defining Euler angles to represent the orientation of a mobile frame of reference. Finally, axis 2 is introduced as the normal of the plane formed by axes 1 and 3. Throughout the article, we treat the thin disklike particle as an oblate spheroid with very small aspect ratio $m = l/d$ (where l is the length of axis 3 and d the length of axis 1 or 2). All the physical parameters are defined according to an oblate spheroid rather than a very thin cylindrical disk.

To relate the instantaneous polarization $\boldsymbol{P}^{\infty}$ and the equilibrium polarization $\boldsymbol{P}^{0}$ to the external field $\boldsymbol{E}_0$, the corresponding high frequency and static polarizabilities (χ_i^{∞} and χ_i^{0}) are introduced, i.e., $P_i^{\infty} = \chi_i^{\infty} E_i$ and $P_i^{0} = \chi_i^{0} E_i$. The electric fields along the three directions are $E_1 = 0$, $E_2 = E_0 \sin\theta$, and $E_3 = E_0 \cos\theta$, respectively. The polarizabilities are defined as

$$\chi_i^{\infty} = \varepsilon_f \frac{\varepsilon_p - \varepsilon_f}{\varepsilon_f + L_i(\varepsilon_p - \varepsilon_f)}, \quad \chi_i^{0} = \varepsilon_f \frac{\sigma_p - \sigma_f}{\sigma_f + L_i(\sigma_p - \sigma_f)},$$

where ε and σ denote the permittivity and conductivity, respectively, the subscript p and f stand for the particle and the surrounding fluid, respectively, and L_i is the depolarization factor along a certain axis i of the ellipsoid ($i = 1,2,3$). The Maxwell-Wagner relaxation time τ_i characterizing the free-charge relaxation is defined as

$$\tau_i = \frac{\varepsilon_f + L_i(\varepsilon_p - \varepsilon_f)}{\sigma_f + L_i(\sigma_p - \sigma_f)}.$$

It is worth noting that for an oblate spheroid with very small aspect ratio ($m \ll 1$) the depolarization factor satisfies $L_1 = L_2 \ll 1$ and $L_3 \approx 1$. For simplicity's sake, one can neglect the depolarization effect in the plane of the disk by setting $L_1 = L_2 = 0$ and $L_3 = 1$. In this limit, the aspect ratio m is eliminated from the analysis of the interfacial polarization dynamics.

Due to the symmetry of the particle, one can define directions parallel and perpendicular to the axis of symmetry (axis 3) as illustrated in Fig. 1(d) and use the subscripts $\parallel$ and $\perp$ instead of 1, 2, and 3 to denote depolarization factors, polarizabilities, and relaxation times along different directions. All the physical parameters needed to define the dynamics of the polarization relaxation are summarized as follows:

$$L_{1,2,\perp} = 0, \quad L_{3,\parallel} = 1, \tag{1}$$

$$\chi^{\infty}_{1,2,\perp} = \varepsilon_f\left(\frac{\varepsilon_p}{\varepsilon_f} - 1\right), \quad \chi^{\infty}_{3,\parallel} = \varepsilon_f\left(1 - \frac{\varepsilon_f}{\varepsilon_p}\right), \tag{2}$$

$$\chi^{0}_{1,2,\perp} = \varepsilon_f\left(\frac{\sigma_p}{\sigma_f} - 1\right), \quad \chi^{0}_{3,\parallel} = \varepsilon_f\left(1 - \frac{\sigma_f}{\sigma_p}\right), \tag{3}$$

$$\tau_{1,2,\perp} = \frac{\varepsilon_f}{\sigma_f}, \quad \tau_{3,\parallel} = \frac{\varepsilon_p}{\sigma_p}. \tag{4}$$

With all the above definitions, the dynamic equations for the retardation polarization can be written as [14]

$$\frac{\partial}{\partial t}P_1^r = -\frac{1}{\tau_\perp}P_1^r - \Omega P_2^r, \tag{5}$$

$$\frac{\partial}{\partial t}P_2^r = -\frac{1}{\tau_\perp}\left[P_2^r + \left(\chi^{\infty}_{\perp} - \chi^{0}_{\perp}\right)E_0\sin\theta\right] + \Omega P_1^r, \tag{6}$$

$$\frac{\partial}{\partial t}P_3^r = -\frac{1}{\tau_\parallel}\left[P_3^r + \left(\chi^{\infty}_{\parallel} - \chi^{0}_{\parallel}\right)E_0\cos\theta\right]. \tag{7}$$

Here $\boldsymbol{\Omega}$ is the angular velocity, which is a vector parallel to axis 3 as illustrated in Fig. 1, and is related to the retardation polarization and angle θ as [14]

$$\Omega = \frac{E_0 P_1^r V}{\Gamma \sin\theta} = \frac{E_0 P_1^r}{\gamma \sin\theta}, \tag{8}$$

where $\Gamma = 4\eta d^3/3$ is the rotational drag coefficient of a thin oblate spheroid, η is the viscosity of the fluid, d is the length of the axis perpendicular to the axis of the symmetry, l is the length of the axis of symmetry, and $V = \pi d^2 l/6$ is the particle volume. For simplicity, one can introduce $\gamma = \Gamma/V = 8\eta/\pi m$ as the rotational drag coefficient per unit volume, where m is the aspect ratio of the oblate spheroid as introduced above. Typically, one needs to introduce rotational drag coefficients with respect to the axis perpendicular and parallel to the symmetry axis 3 respectively for a disk. However, we are only interested in a nanometer-thin disk whose aspect ratio satisfies $m \ll 1$. The two drag coefficients are approximately equal in that limit. (See Appendix A for details.)

If $\Omega = 0$, the dynamics of the retardation polarization $\boldsymbol{P}^r$ is governed by the Maxwell-Wagner relaxation time [see Eqs. (5)–(7)], i.e., $\partial P_i^r/\partial t = -(P_i^r + P_i^{\infty} - P_i^0)/\tau_i$, as discussed above. The charge relaxation solely relies on the conduction current (current driven by electric field). When the particle starts to spin, the spinning motion induces convection current and an additional term $\boldsymbol{\Omega}\times\boldsymbol{P}^r$ must be added as shown on the right-hand side of Eqs. (5) and (6). Finally, in the limits of low Reynolds number, the angle θ defining the orientation of the disk with respect to the field E_0 satisfies the following dynamic equation [14]:

$$\gamma\dot{\theta} = [(\boldsymbol{P}^r + \boldsymbol{P}^{\infty}) \times \boldsymbol{E}]_1 = \tfrac{1}{2}\left(\chi^{\infty}_{\perp} - \chi^{\infty}_{\parallel}\right)E_0^2\sin 2\theta + P_2^r E_0\cos\theta - P_3^r E_0\sin\theta. \tag{9}$$

By substituting Eq. (8) into Eqs. (5) and (6), one can have a closed set of equations (5)–(7) and (9) describing the dynamics of the Quincke rotation.

TABLE I. Conditions for stable steady states of oblate spheroids.

States	Cases	Stability
Nonspinning	$C_1 < 0$	always stable
	$C_1 > 0,\ C_2 < 0$	only stable if $E_0^2 < C_1$
	$C_2 > 0$	only stable if $E_0^2 < \min(C_1, C_2)$
Spinning	$C_1 > 0$	only stable if $E_0^2 > \max(C_1, C_3)$
	$C_1 < 0$	no stable spinning state possible

III. STABILITY AND CRITICAL FIELD

A. Steady states and their stabilities

The full analysis of the dynamic system defined by Eqs. (5)–(7) and (9) requires solving the differential equations numerically with a defined initial condition. In this paper we only focus on analyzing the possible steady states (including steady orientation and rotation) and their stabilities so that one can find a window of parameters to practically control the orientation or rotation of the particle. To achieve a steady state, all the time derivatives must be set to zero, i.e., $\partial P_i^r/\partial t$ and $\dot{\theta} = 0$ in Eqs. (5)–(7) and (9). Given the symmetry of the system, there are two possible scenarios regarding the particle orientation at the stationary state with respect to the field, i.e., (i) $\theta = 0$ and (ii) $\theta = \pi/2$.

As for scenario (i) $\theta = 0$, at stationary state, one can immediately find that $P_2^r = 0$ from Eq. (9) and then $P_1^r = 0$ from Eq. (5) and $P_3^r = (\chi_\parallel^0 - \chi_\parallel^\infty)E_0$ from Eq. (7). By checking the eigenvalues of the Jacobian matrix, this stationary point is confirmed to be always unstable (Appendix B). Therefore, in a stable equilibrium, the axis of symmetry of a disk cannot be parallel to the electric field. This is understandable from a thermodynamics perspective since this particular configuration results in a greater depolarization field and higher electrostatic energy as compared to the case $\theta = \pi/2$ when the axis of symmetry is perpendicular to the electric field.

As for scenario (ii) $\theta = \pi/2$, Eq. (7) yields $P_3^r = 0$. The two remaining variables can be solved from Eqs. (5) and (6):

$$P_2^r = -\frac{(\chi_\perp^\infty - \chi_\perp^0)E_0}{\tau_\perp^2\Omega^2 + 1}, \quad P_1^r = -\Omega\tau_\perp P_2^r. \tag{10}$$

If $\Omega = 0$, then $P_1^r = 0$ and $P_2^r = (\chi_\perp^0 - \chi_\perp^\infty)E_0$. This corresponds to a nonspinning orientation state with the axis of symmetry perpendicular to the electric field. There will be two critical values to define the stability of this state (Appendix B),

$$C_1 = \frac{\gamma}{(\chi_\perp^\infty - \chi_\perp^0)\tau_\perp} = \frac{C_0}{\varepsilon_p/\varepsilon_f - \sigma_p/\sigma_f}, \tag{11}$$

$$C_2 = \frac{\gamma}{(\chi_\parallel^\infty - \chi_\perp^0)\tau_\parallel} = \frac{\varepsilon_f}{\varepsilon_p}\frac{\sigma_p}{\sigma_f}\frac{C_0}{2 - \sigma_p/\sigma_f - \varepsilon_f/\varepsilon_p}, \tag{12}$$

where the parameter C_0 is defined as

$$C_0 = \frac{\gamma}{\tau_\perp\varepsilon_f} = \frac{8\eta\sigma_f}{\pi\varepsilon_f^2}\frac{d}{l}. \tag{13}$$

The conditions for a stable nonspinning orientation state is summarized in Table I. The critical values and the related conditions for stable orientation are found by calculating the eigenvalues of the Jacobian matrix (Appendix B).

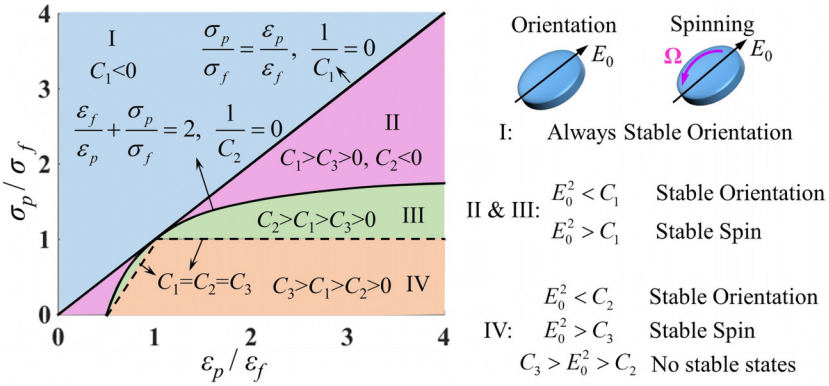

FIG. 2. Phase diagram characterizing the stabilities of both the nonspinning orientation and spinning states. In region I, the disk surface is always parallel to the external electric field. In regions II and III, depending on the strength of the electric field, the disk may be in a stable orientation state ($E_0 < C_1^{0.5}$) or a spinning state ($E_0 > C_1^{0.5}$). In region IV, if $E_0 < C_2^{0.5}$, the orientation state is stable. If $E_0 > C_3^{0.5}$, the spinning state is stable. The dynamical system might end up with a limit cycle or just chaos if the electric field satisfies $C_3^{0.5} > E_0 > C_2^{0.5}$. The parameters C_1, C_2, and C_3 can be found in Eqs. (11), (12), and (15).

If $\Omega \neq 0$, the particle is spinning around its axis of symmetry and the angular velocity Ω can be found by combining Eqs. (8) and (10):

$$\Omega^2 = \frac{1}{\tau_\perp^2}\left(E_0^2/C_1 - 1\right). \tag{14}$$

Obviously, the right-hand side of Eq. (14) has to be positive to have a real-valued angular velocity Ω. This condition can be interpreted as $C_1 > 0$ and $E_0^2 > C_1$. Meanwhile, the stationary point can be found as $P_1^r = \Omega\gamma/E_0$, $P_2^r = -\gamma/(E_0\tau_\perp)$, $P_3^r = 0$, and $\theta = \pi/2$. The stability of the spinning states is determined by the following critical values (Appendix B):

$$C_3 = \gamma\left(\frac{1}{\tau_\perp} - \frac{1}{\tau_\parallel}\right)\frac{1}{\chi_\perp^\infty - \chi_\parallel^\infty} = \left(1 - \frac{\varepsilon_f}{\varepsilon_p}\frac{\sigma_p}{\sigma_f}\right)\frac{C_0}{\varepsilon_p/\varepsilon_f + \varepsilon_f/\varepsilon_p - 2}. \tag{15}$$

The condition for a stable spinning state is found to be $E_0^2 > C_3$ (Appendix B). Together with the condition to have a real-valued angular velocity Ω, the requirements for realizing Quincke rotation of a thin disk are summarized as $E_0^2 > \max(C_1, C_3)$ and $C_1 > 0$ (Table I). It is worth noting that, results illustrated in Table I are not only limited to thin disks ($m \ll 1$) but are also applicable for any oblate spheroids whose aspect ratio m is less than 1. The related parameters C_1, C_2, and C_3 are defined by Eqs. (B7), (B9), and (B15) (Appendix B) for an arbitrary oblate spheroid. Conditions regarding the stability of the steady states for both prolate and oblate spheroids can also be found in Table II (Appendix B). As can be seen from Eqs. (11), (12), and (15), if one normalizes C_1, C_2, and C_3 with C_0, the relative permittivity $\varepsilon_p/\varepsilon_f$ and the relative conductivity σ_p/σ_f completely determine these three critical values. This allow us to construct a master phase diagram in terms of the material parameters to better illustrate the stabilities of the nonspinning orientation and spinning states.

The phase diagram and the corresponding regions characterizing the stabilities are illustrated in Fig. 2. Based on Table I, the necessary separatrices should include the lines where C_1 and C_2 flip their signs (solid lines in Fig. 2) as well as the lines along which $C_1 = C_3$ or $C_1 = C_2$ (dashed lines in Fig. 2; $C_1 = C_3$ and $C_1 = C_2$ share the same line).

In region IV, no stable states can be achieved if the electric field satisfies $C_3 > E_0^2 > C_2$. In this special case, the dynamic system would end up with a limit cycle or just chaos [24]. Discussions about those dynamical behaviors are beyond the scope of this work, therefore only the stable states

will be analyzed. Except for this particular case, the nanodisk will be either a nonspinning orientation state or a spinning state. Figure 2 shows that the bistability observed in a prolate spheroid [14] is impossible for a disklike particle, indicating that no hysteresis will occur when the system undergoes a transition between the two stable states (orientation and spinning). This allows one to control the state of the dynamic system without worrying about its history. The absence of bistability can be explained as follows. For an oblate spheroid, the axis of symmetry is perpendicular to the electric field in both nonspinning and spinning states. If the nonspinning orientation state is stable, no matter how significant the in-plane disturbance is, e.g., a large in-plane rotation, the disk will always settle down to the new orientation state, which is essentially the same as the original one due to the particle symmetry. Therefore, no in-plane perturbation can induce spontaneous rotation in this case and the spinning state is only possible if the nonspinning orientation state becomes unstable, while for a prolate spheroid the axis of symmetry forms different angles with the electric field in nonspinning ($\theta = 0$) and spinning states ($\theta = \pi/2$). Therefore, a large perturbation might kick off the particle from the stable orientation state ($\theta = 0$) to the stable spinning state ($\theta = \pi/2$) and a bistability is possible.

Moreover, unlike the prolate spheroid case in which the spinning state loses its stability if the electric field is greater than a critical value [13,14], there is no such upper limit of the electric field for disklike particles. Therefore, as indicated by Eq. (14), the nanometer-thin disk can spin at any speed (within the low-Reynolds-number limit) as long as the external electric field will not break down the material or the surrounding fluid.

B. Critical field

As discussed above and illustrated in Fig. 2, to achieve a stable spinning state, the electric field has to be greater than a critical value, i.e., $E_0 > E_c$, where $E_c^2 = \max(C_1, C_3)$. It is important to keep E_c reasonably low, otherwise the material might break down before the electric field E_0 reaches the critical value E_c. As shown by Eqs. (11) and (15), E_c scales with $(C_0)^{0.5}$, which depends on the fluid properties and the aspect ratio of the disk. For a nanometer-thin disk, d/l is typically greater than 10^2. If we consider a fluid with viscosity approximately 10^{-3} Pa s, conductivity $10^{-9}(\Omega\,\mathrm{m})^{-1}$, and permittivity approximately 10^{-11} F/m, the estimated critical electric field E_c is on the order of 10^6 V/m, which is already approaching the breakdown electric-field strength of most materials. Therefore, the selection of the fluid is pivotal for realization of Quincke rotation for disklike particles and Eq. (11) gives a pretty good order of magnitude estimation of the critical field.

An accurate calculation of the normalized critical fields $E_c/(C_0)^{0.5}$ is shown in Fig. 3 (color is in logarithmic scale), which provides guidance on experimental selection of materials for Quincke rotation. It becomes clear that in order to realize Quincke rotation at a reasonably strong electric field, one has to stay away from two lines: $\varepsilon_p/\varepsilon_f = 1$ (C_3 tends to infinity) and $\varepsilon_p/\varepsilon_f = \sigma_p/\sigma_f$ (C_1 tends to infinity). Meanwhile, materials with larger permittivity ε_p are in favor of Quincke rotation as it results in a lower critical field and provides more freedom to tune the conductivity with light within the rotation region. In a real experiment, one can consider all the parameters to be fixed except for the conductivity of the disk. Therefore, the minimum field required for the Quincke rotation to be possible can be defined for a certain $\varepsilon_p/\varepsilon_f$. If the external electric field is smaller than this value, the disk will not spin no matter how one tunes its conductivity with light. This minimum field sits on the dashed lines in Fig. 3 and is plotted in the inset. It reemphasizes that one should never approach $\varepsilon_p/\varepsilon_f = 0$ or $\varepsilon_p/\varepsilon_f = 1$ as the minimum critical field tends to infinity in the vicinity of those two lines.

IV. OPTICAL TUNABILITY

In optoelectronics, the electric conductivity of a photoconductor typically increases linearly with the incident light intensity I, i.e., $\sigma_p = \sigma_d + \alpha I$, where σ_d is the dark conductivity and α ($\alpha > 0$) is the coefficient that relates the light intensity to the photoconductivity. The increase of conductivity is commonly attributed to the photogenerated free-charge carriers, i.e., the free-charge density is higher

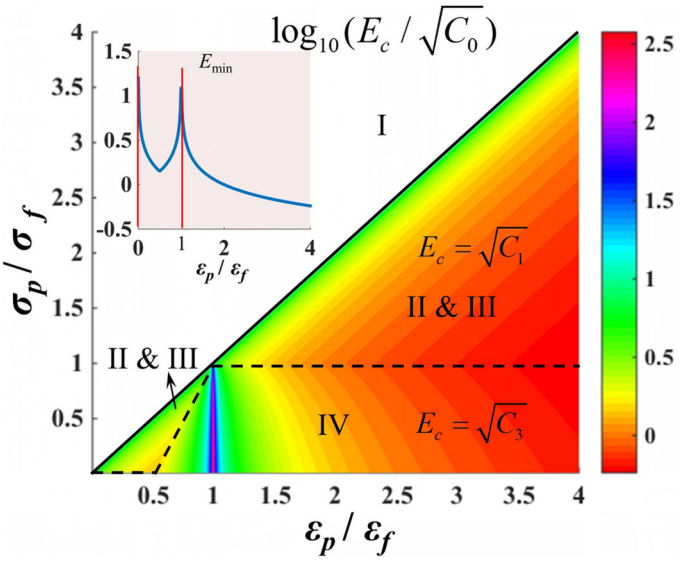

FIG. 3. Critical electric field to have stable Quincke rotation. The color is in logarithm scale representing $\log_{10}[E_c/(C_0)^{0.5}]$. The solid line separates region I, where Quincke rotation is impossible, from regions II–IV where the rotation is possible. Dashed lines separate regions II and III, where the critical field is $(C_1)^{0.5}$, from region IV, where critical field is $(C_3)^{0.5}$. The inset corresponds to the critical field along the dashed line, which stands for the minimum electric field required at a certain $\varepsilon_p/\varepsilon_f$ if σ_p/σ_f can be tuned in the full range. The curve approaches the two vertical red lines asymptotically.

than that of the dark state. Since the permittivity of a material is determined by the displacement of bound charged elements rather than free charges, light will not change the permittivity of the disk in most cases. Therefore, by increasing the light intensity, one gradually moves from the lower part to the upper part of Fig. 3 along a line perpendicular to the horizontal axis. We assume that $\sigma_p/\sigma_f \ll 1$ when light is off and the permittivity satisfies $\varepsilon_p/\varepsilon_f > 1$. Since the critical field reaches a minimum when $\sigma_p/\sigma_f = 1$ (see Fig. 3), the effects of light will be twofold. First, it might induce the spinning of an initially nonspinning sample, i.e., $E_0 < (C_3)^{1/2}$, since the critical field $(C_3)^{1/2}$ decreases with light intensity when $\sigma_p/\sigma_f < 1$. Second, for an already spinning disk, the spin will eventually stop if the light is sufficiently strong that the critical field $(C_1)^{1/2}$ becomes greater than the external field E_0. To further illustrate the optical tunability of Quincke rotation, we calculate the spinning speed of a Quincke rotor as

$$\Omega = \frac{\sigma_f}{\varepsilon_f}\sqrt{\frac{\pi\varepsilon_f^2 E_0^2}{8\eta\sigma_f}\frac{l}{d}\left(\frac{\varepsilon_p}{\varepsilon_f}-\frac{\sigma_p}{\sigma_f}\right)-1}. \tag{16}$$

It is obtained by substituting Eqs. (4), (11), and (13) into Eq. (14). It appears that the spinning speed scales with $1/\tau_f = \sigma_f/\varepsilon_f$ (τ_f is the charge relaxation time of the fluid), which is independent of the material properties of the particle used in the experiment. The reason lies in the fact that, for a very thin disk, the depolarization factor $L_\perp$ is zero when the electric field is perpendicular to the particle's axis of symmetry (the configuration for the spinning state). Therefore, the electric field inside the material is the same as the external field and the presence of the particle does not introduce any disturbance of the field distribution as if the material does not exist. This is unique for a thin disk as the Maxwell-Wagner relaxation time $\tau_\perp$ depends on both fluid and particle properties for either a sphere or prolate spheroid.

Figures 4(a) and 4(b) are the contours of spinning velocity Ω as a function of electric field and relative conductivity (light intensity) for two different relative permittivities ($\varepsilon_p/\varepsilon_f = 2$ and 25,

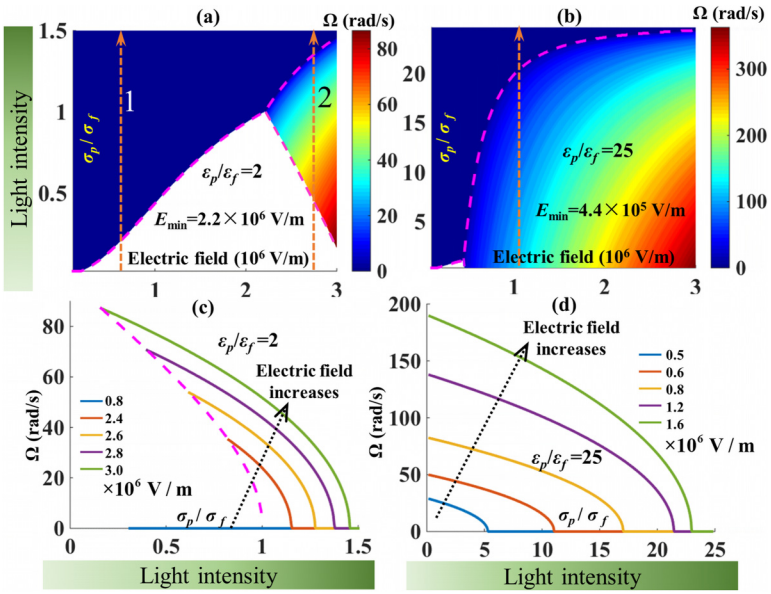

FIG. 4. (a) and (b) Contour of the spinning speed as a function of external electric field and the relative conductivity (light intensity). The relative conductivity σ_p/σ_f is very low when the light is off and gradually increases as the light intensity increases. The relative permittivities are $\varepsilon_p/\varepsilon_f = 2$ and 25, respectively. (c) and (d) Illustration of tuning the rotation speed Ω with light. The physical parameters used for the calculation are $l = 5\,\text{nm}$, $d = 3\,\mu\text{m}$, $\varepsilon_f = 2\varepsilon_0$, $\sigma_f = 10^{-9}\,(\Omega\,\text{m})^{-1}$, $\eta = 10^{-3}\,\text{Pa s}$.

respectively). The zero-spinning-speed region (dark blue) corresponds to the stable orientation state and the white region is where no stable stationary states exist and the spinning speed is not defined. It shows that larger $\varepsilon_p/\varepsilon_f$ results in a smaller unstable region as well as higher spinning speed under the same electric field. To achieve a really high spinning speed, one must try reaching the lower right corner of the graph to have a small σ_p/σ_f and large electric field as indicated by Eq. (16). Meanwhile, the optical tunability is also illustrated by the dashed arrow lines along which the light intensity gradually increases. For $\varepsilon_p/\varepsilon_f = 2$, the disk initially sits in the white area where no stable states exist [Fig. 4(a)]. As the light intensity increases, the disk may or may not go through the Quincke rotation region, depending on the strength of the electric field. The electric field must be greater than $E_{\text{min}} = 2.2\times10^6\,\text{V/m}$ to ensure that the disk will starts to spin at some point [line 2 in Fig. 4(a)] rather than directly settle down to a spinless orientation state [line 1 in Fig. 4(a)]. For $\varepsilon_p/\varepsilon_f = 25$, the disk is initially spinning and the spinning speed gradually decreases to zero as the light intensity increases [Fig. 4(b)]. Figures 4(c) and 4(d) illustrate the optical tunability more clearly.

V. CONCLUSION

We proposed an optically tunable Quincke rotation of disklike particles. The instability analysis of the dynamical system suggests no bistability and the particle's dynamic behavior can be controlled by the relative permittivity, conductivity, and external electric field (Fig. 2). Therefore, one can use light to switch between the spinning state and nonspinning orientation state by varying the conductivity of the particle. The effect of light is twofold: It may jumpstart the rotation of an initially nonspinning disk or slow down the rotation of a spinning disk. Moreover, a large $\varepsilon_p/\varepsilon_f$ results in a small critical field E_c, which is in favor of realizing Quincke rotation and also allows more freedom for tuning the rotation with light. We believe this theoretical work clarifies the instability of the Quincke rotation for disklike particles and will help guide the experimental realization of an optically tunable Quincke rotor or other types of nanomotors.

ACKNOWLEDGMENTS

This work was financially supported by National Key R&D Program of China (Grant No. 2017YFA0305500), National Natural Science Foundation of China (Grant No. 11604152), Fundamental Research Funds for the Central Universities (Grants No. 30915012205 and No. 30916015106), Natural Science Foundation of Jiangsu Province (Grants No. BK20160815 and No. BK20140769), PAPD of Jiangsu Higher Education Institutions. We also acknowledge Computer Network Information Center (Supercomputing Center) of Chinese Academy of Sciences for allocation of computing resources.

APPENDIX A: DRAG COEFFICIENT OF A THIN DISK

The rotational drag coefficient Γ of a particle determines the angular velocity Ω in response to an external torque M, i.e., $\Omega = M/\Gamma$. This value depends on both the particle shape and size. For a sphere, $\Gamma = 8\pi\eta R^3 = 6\eta V$ [25], where R is the radius of the sphere, V is the particle volume, and η is the viscosity of the fluid. For a spheroid, one needs to use the aspect ratio $m = l/d$ to define the particle shape. Here l is the length of the axis of symmetry and d is the length of the axis perpendicular to it. The rotational drag coefficient is typically defined through the Perrin factor f, which is the multiplicative adjustment to the rotational friction of a rigid spheroid, relative to the corresponding friction in spheres of the same volume. Therefore, the rotational drag coefficient for a spheroid can be defined as $6\eta f V$, which is proportional to the particle volume. To simplify the notation, one can introduce the rotational drag coefficient per unit volume as $6\eta f$.

The rotational Perrin factor for an oblate spheroid ($m < 1$) is defined as [26]

$$f_{\parallel} = \frac{2}{3m}\frac{(1-m^2)^{3/2}}{\arctan(\sqrt{m^{-2}-1}) - m\sqrt{1-m^2}}, \tag{A1}$$

$$f_{\perp} = \frac{2}{3m}\frac{(1+m^2)(1-m^2)^{3/2}}{(1-2m^2)\arctan(\sqrt{m^{-2}-1}) + m\sqrt{1-m^2}}. \tag{A2}$$

The subscript $\parallel$ stands for the rotation with respect to the axis of symmetry and $\perp$ stands for the rotation with respect to any axis perpendicular to the axis of symmetry. Therefore, the rotational drag coefficient of a certain oblate spheroid normalized by the particle volume is defined as

$$\gamma_{\parallel,\perp} = 6\eta f_{\parallel,\perp} = 6\eta f_{\parallel,\perp}. \tag{A3}$$

In the case of a very thin disk ($m \ll 1$), the following relation holds true:

$$\arctan(\sqrt{m^{-2}-1}) = \frac{\pi}{2} + \frac{1}{1+m^{-2}-1}\frac{1}{2\sqrt{m^{-2}-1}}\frac{-2}{m^3}\bigg|_{m=0} m = \frac{\pi}{2} - m.$$

Therefore, the Perrin factor can be expanded as

$$f_{\parallel} \approx \frac{2}{3m}\frac{1}{\frac{\pi}{2}-m-m} = \frac{4}{3m\pi}\frac{1}{1-4m/\pi} \approx \frac{4}{3m\pi},$$

$$f_{\perp} \approx \frac{2}{3m}\frac{1}{\frac{\pi}{2}-m+m} = \frac{4}{3m\pi}.$$

The rotational drag coefficient of a thin disk normalized by its volume satisfies

$$\gamma_{\parallel} \approx \gamma_{\perp} \approx \frac{8\eta}{m\pi}. \tag{A4}$$

APPENDIX B: ANALYSIS OF THE INSTABILITY OF THE DYNAMICAL SYSTEM

To maintain generality, the derivation here does not assume $\gamma_\parallel = \gamma_\perp$, i.e., the result is not limited to a very thin disk but also is applicable to any oblate spheroid. The dynamical system is still defined by Eqs. (5)–(9). Equations (8) and (9) are rewritten in a more general case as

$$\gamma_\perp \dot{\theta} = \tfrac{1}{2}\left(\chi_\perp^\infty - \chi_\parallel^\infty\right) E_0^2 \sin 2\theta + P_2^r E_0 \cos\theta - P_3^r E_0 \sin\theta, \tag{B1}$$

$$\Omega = E_0 P_1^r \left(\frac{\sin\theta}{\gamma_\parallel} + \frac{\cos^2\theta}{\gamma_\perp \sin\theta}\right). \tag{B2}$$

1. Case (i): $\theta = 0$

One can immediately find that the stationary point satisfies $P_2^r = 0$, $P_1^r = 0$, and $P_3^r = (\chi_\parallel^0 - \chi_\parallel^\infty)E_0$. The stability of the stationary point can be analyzed by introducing a small deviation near it, i.e.,

$$\begin{aligned}
\frac{\partial \delta P_1^r}{\partial t} &= -\frac{1}{\tau_\perp}\delta P_1^r, \\
\frac{\partial \delta P_2^r}{\partial t} &= -\frac{1}{\tau_\perp}\delta P_2^r - \frac{1}{\tau_\perp}\left(\chi_\perp^\infty - \chi_\perp^0\right) E_0 \delta\theta, \\
\frac{\partial \delta P_3^r}{\partial t} &= -\frac{1}{\tau_\parallel}\delta P_3^r, \\
\gamma_\perp \delta\dot{\theta} &= \left(\chi_\perp^\infty - \chi_\parallel^0\right) E_0^2 \delta\theta + E_0 \delta P_2^r.
\end{aligned}$$

It becomes clear that P_1^r and P_3^r would always converge to its stationary value and the stability is determined by the Jacobian matrix regarding P_2^r and θ:

$$\begin{pmatrix} -1/\tau_\perp & -\left(\chi_\perp^\infty - \chi_\perp^0\right) E_0/\tau_\perp \\ E_0/\gamma_\perp & \left(\chi_\perp^\infty - \chi_\parallel^0\right) E_0^2/\gamma_\perp \end{pmatrix}.$$

The eigenvalues can be calculated with the following equation:

$$\tau_\perp \gamma_\perp \lambda^2 + \left[\gamma_\perp - \tau_\perp\left(\chi_\perp^\infty - \chi_\parallel^0\right) E_0^2\right]\lambda + \left(\chi_\parallel^0 - \chi_\perp^0\right) E_0^2 = 0.$$

To have a stable solution, the following relations must be satisfied [24]:

$$\gamma_\perp - \tau_\perp\left(\chi_\perp^\infty - \chi_\parallel^0\right) E_0^2 > 0, \quad \left(\chi_{||}^0 - \chi_\perp^0\right) E_0^2 > 0. \tag{B3}$$

The parameter $\chi_\parallel^0 - \chi_\perp^0$ can be expanded as

$$\chi_\parallel^0 - \chi_\perp^0 = \varepsilon_f \frac{(\sigma_p - \sigma_f)^2 (L_\perp - L_{||})}{[\sigma_f + L_\parallel(\sigma_p - \sigma_f)][\sigma_f + L_\perp(\sigma_p - \sigma_f)]}. \tag{B4}$$

Therefore, for a prolate spheroid ($L_\perp > L_\parallel$), this orientation state is stable if one of the two following conditions is satisfied:

$$\chi_\perp^\infty - \chi_\parallel^0 < 0 \quad \text{or} \quad E_0^2 < \frac{\gamma_\perp}{\tau_\perp}\frac{1}{\chi_\perp^\infty - \chi_\parallel^0} = C_{01}. \tag{B5}$$

For an oblate spheroid ($L_\perp < L_\parallel$), the eigenvalues are always real and have opposite signs, indicating that the system is always unstable at this stationary point.

2. Case (ii): $\theta = \pi/2$

Equation (7) yields $P_3^r = 0$. The two remaining variables can be solved as

$$P_2^r = -\frac{(\chi_\perp^\infty - \chi_\perp^0)E_0}{\tau_\perp^2\Omega^2 + 1}, \quad P_1^r = -\Omega\tau_\perp P_2^r. \tag{B6}$$

a. Nonspinning state

If $\Omega = 0$, then $P_1^r = 0$ and $P_2^r = (\chi_\perp^0 - \chi_\perp^\infty)E_0$. This corresponds to a nonspinning orientation state with the axis of symmetry perpendicular to the electric field. Introducing a small deviation near the stationary point yields

$$\begin{aligned}
\frac{\partial \delta P_1^r}{\partial t} &= \left[\frac{(\chi_\perp^\infty - \chi_\perp^0)E_0^2}{\gamma_\parallel} - \frac{1}{\tau_\perp}\right]\delta P_1^r, \\
\frac{\partial \delta P_2^r}{\partial t} &= -\frac{1}{\tau_\perp}\delta P_2^r, \\
\frac{\partial \delta P_3^r}{\partial t} &= -\frac{1}{\tau_\parallel}\left[\delta P_3^r - (\chi_\parallel^\infty - \chi_\parallel^0)E_0\delta\theta\right], \\
\gamma_\perp \delta\dot{\theta} &= (\chi_\parallel^\infty - \chi_\perp^0)E_0^2\delta\theta - E_0\delta P_3^r.
\end{aligned}$$

The solution for P_2^r is always stable. A stable solution for P_1^r requires one of the two following conditions:

$$\chi_\perp^\infty - \chi_\perp^0 < 0 \quad \text{or} \quad E_0^2 < \frac{\gamma_\parallel}{(\chi_\perp^\infty - \chi_\perp^0)\tau_\perp} = C_1. \tag{B7}$$

The Jacobian matrix regarding P_3^r and θ is written as

$$\begin{pmatrix} -1/\tau_{||} & (\chi_{||}^\infty - \chi_{||}^0)E_0/\tau_{||} \\ -E_0/\gamma_\perp & (\chi_{||}^\infty - \chi_\perp^0)E_0^2/\gamma_\perp \end{pmatrix}.$$

The eigenvalues can be calculated with the following equation:

$$\gamma_\perp\tau_\parallel\lambda^2 + \left[\gamma_\perp - (\chi_\parallel^\infty - \chi_\perp^0)\tau_\parallel E_0^2\right]\lambda + (\chi_\perp^0 - \chi_\parallel^0)E_0^2 = 0.$$

To have a stable solution, the following relations must be satisfied:

$$\gamma_\perp - (\chi_\parallel^\infty - \chi_\perp^0)\tau_\parallel E_0^2 > 0, \quad (\chi_\perp^0 - \chi_\parallel^0)E_0^2 > 0. \tag{B8}$$

Following Eq. (B4), $\chi_\perp^0 - \chi_\parallel^0 > 0$ is always satisfied for an oblate spheroid and $\chi_\perp^0 - \chi_\parallel^0 < 0$ always holds true for a prolate spheroid. Therefore, the stable nonspinning state for a prolate spheroid is impossible for this orientation. For an oblate spheroid, a stable orientation requires

$$\chi_{||}^\infty - \chi_\perp^0 < 0 \quad \text{or} \quad E_0^2 < \frac{\gamma_\perp}{(\chi_\parallel^\infty - \chi_\perp^0)\tau_\parallel} = C_2. \tag{B9}$$

Meanwhile, with the help of Eqs. (B7) and (B9), the following relation can be proven for an oblate spheroid:

$$\begin{aligned}
\frac{\gamma_\parallel}{\tau_\perp}\frac{1}{C_1} - \frac{\gamma_\perp}{\tau_\parallel}\frac{1}{C_2} &= (\chi_\perp^\infty - \chi_\perp^0) - (\chi_\parallel^\infty - \chi_\perp^0) = \chi_\perp^\infty - \chi_\parallel^\infty \\
&= \varepsilon_f \frac{(\varepsilon_p - \varepsilon_f)^2(L_\parallel - L_\perp)}{[\varepsilon_f + L_\perp(\varepsilon_p - \varepsilon_f)][\varepsilon_f + L_\parallel(\varepsilon_p - \varepsilon_f)]} > 0.
\end{aligned} \tag{B10}$$

Therefore, if $C_1 < 0$, then $C_2 < 0$ and if $C_2 > 0$ then $C_1 > 0$. The condition for stable orientation state can be summarized as follows:

$$\begin{aligned} &C_1 < 0 \quad \text{(always stable)},\\ &C_2 > 0 \quad \left[\text{stable if } E_0^2 < \min(C_1, C_2)\right],\\ &C_1 > 0, \quad C_2 < 0 \quad \left(\text{stable if } E_0^2 < C_1\right). \end{aligned} \tag{B11}$$

For a general spheroid,

$$\frac{\gamma_\parallel}{\tau_\perp}\frac{1}{C_1} = \chi_\perp^\infty - \chi_\perp^0 = \varepsilon_f \frac{(\varepsilon_p\sigma_f - \sigma_p\varepsilon_f)}{[\varepsilon_f + L_\perp(\varepsilon_p - \varepsilon_f)][\sigma_f + L_\perp(\sigma_p - \sigma_f)]}. \tag{B12}$$

Therefore, the sign of this parameter relies on the material property rather than the particle geometry. All the spheroids share the same condition for C_1 to flip its sign.

b. Spinning case

The nonzero Ω can be calculated by combining Eqs. (B2) and (B6):

$$\Omega^2 = \frac{1}{\tau_\perp^2}\left(E_0^2/C_1 - 1\right). \tag{B13}$$

For this state to exist,

$$E_0^2 > C_1 > 0. \tag{B14}$$

The stationary point satisfies Eq. (B6). Together with $\theta = \pi/2$, $P_3^r = 0$ and Eq. (B2), one can write the stationary point as

$$P_1^r = \frac{\gamma_\parallel}{E_0}\Omega, \quad P_2^r = -\frac{\gamma_\parallel}{E_0}\frac{1}{\tau_\perp}, \quad P_3^r = 0, \quad \theta = \pi/2.$$

Meanwhile, the angular velocity satisfies

$$\delta\Omega = \frac{E_0}{\gamma_\parallel}\delta P_1^r.$$

Introducing a small deviation near the stationary point yields

$$\begin{aligned} \frac{\partial\delta P_1^r}{\partial t} &= -\Omega\delta P_2^r,\\ \frac{\partial\delta P_2^r}{\partial t} &= -\frac{1}{\tau_\perp}\delta P_2^r + 2\Omega\delta P_1^r,\\ \frac{\partial\delta P_3^r}{\partial t} &= -\frac{1}{\tau_\parallel}\left[\delta P_3^r - \left(\chi_\parallel^\infty - \chi_\parallel^0\right)E_0\delta\theta\right],\\ \gamma_\perp\delta\dot{\theta} &= \left[\left(\chi_\parallel^\infty - \chi_\perp^\infty\right)E_0^2 + \frac{\gamma_\parallel}{\tau_\perp}\right]\delta\theta - E_0\delta P_3^r. \end{aligned}$$

The Jacobian matrix for the dynamical system regarding P_1^r and P_2^r is written as

$$\begin{pmatrix} 0 & -\Omega \\ 2\Omega & -1/\tau_\perp \end{pmatrix}.$$

Its eigenvalue is determined by

$$\lambda^2 + \lambda/\tau_\perp + 2\Omega^2 = 0.$$

It is obvious that the real part of the two eigenvalues is always negative. Therefore, P_1^r and P_2^r always converge to its stationary value.

The Jacobian matrix for the dynamical system regarding P_3^r and θ is written as

$$\begin{pmatrix} -\frac{1}{\tau_\parallel} & \frac{\chi_\parallel^\infty - \chi_\parallel^0}{\tau_\parallel} E_0 \\ -\frac{E_0}{\gamma_\perp} & \frac{\chi_\parallel^\infty - \chi_\perp^\infty}{\gamma_\perp} E_0^2 + \frac{\gamma_\parallel}{\gamma_\perp}\frac{1}{\tau_\perp} \end{pmatrix}.$$

Its eigenvalue is calculated by

$$\lambda^2 + \left(\frac{1}{\tau_\parallel} - \frac{\chi_\parallel^\infty - \chi_\perp^\infty}{\gamma_\perp} E_0^2 - \frac{\gamma_\parallel}{\gamma_\perp}\frac{1}{\tau_\perp}\right)\lambda + \frac{\chi_\perp^\infty - \chi_\parallel^0}{\tau_\parallel \gamma_\perp} E_0^2 - \frac{\gamma_\parallel}{\gamma_\perp}\frac{1}{\tau_\perp \tau_\parallel} = 0.$$

Therefore, the conditions for the spinning state to be stable are interpreted as

$$\tau_\perp \tau_\parallel \left(\chi_\perp^\infty - \chi_\parallel^\infty\right) E_0^2 + \gamma_\perp \tau_\perp - \gamma_\parallel \tau_\parallel > 0,$$
$$\tau_\perp \left(\chi_\perp^\infty - \chi_\parallel^0\right) E_0^2 - \gamma_\parallel > 0.$$

From Eq. (B10) one can find that $\chi_\perp^\infty - \chi_\parallel^\infty > 0$ for an oblate spheroid and $\chi_\perp^\infty - \chi_\parallel^\infty < 0$ for a prolate spheroid. Therefore, the first condition for a stable spinning state becomes

$$E_0^2 > \left(\frac{\gamma_\parallel}{\tau_\perp} - \frac{\gamma_\perp}{\tau_\parallel}\right)\frac{1}{\chi_\perp^\infty - \chi_\parallel^\infty} = C_3 \quad \text{(oblate spheroid)},$$
$$E_0^2 < \left(\frac{\gamma_\parallel}{\tau_\perp} - \frac{\gamma_\perp}{\tau_\parallel}\right)\frac{1}{\chi_\perp^\infty - \chi_\parallel^\infty} = C_3 \quad \text{(prolate spheroid)}. \tag{B15}$$

The other condition would be

$$\chi_\perp^\infty - \chi_\parallel^0 > 0, \quad E_0^2 > \frac{\gamma_{||}}{\left(\chi_\perp^\infty - \chi_\parallel^0\right)\tau_\perp} = C_4.$$

Together with Eq. (B7), one can easily prove that

$$\frac{1}{C_4} - \frac{1}{C_1} = \frac{\tau_\perp}{\gamma_\parallel}\left[\left(\chi_\perp^\infty - \chi_\parallel^0\right) - \left(\chi_\perp^\infty - \chi_\perp^0\right)\right] = \frac{\tau_\perp}{\gamma_\parallel}\left(\chi_\perp^0 - \chi_\parallel^0\right).$$

According to Eq. (B4), $\chi_\perp^0 - \chi_\parallel^0$ is positive for an oblate spheroid and $\chi_\perp^0 - \chi_\parallel^0$ is negative for a prolate spheroid. Therefore, one can remove C_4 from the discussion for an oblate spheroid as $E_0^2 > C_4$ will be automatically satisfied if $E_0^2 > C_1 > 0$ is satisfied, which is required for a spinning state to exist [Eq. (B13)]. Therefore, together with Eq. (B15) the condition for a stable spinning state to exist for an oblate spheroid can be summarized as

$$C_1 > 0, \quad E_0^2 > \max(C_1, C_3). \tag{B16}$$

For a prolate spheroid, C_1, C_3, and C_4 must all be positive. Under this condition $C_4 > C_1$ is automatically satisfied. The condition for the stable spinning state can be summarized as

$$C_1 > 0, \quad C_3 > C_4 > 0, \quad C_3 > E_0^2 > C_4. \tag{B17}$$

3. Summary of conditions and the thin disk approximation

The stability of the steady states of both prolate and oblate spheroids is summarized in Table II. The related parameters are defined as

$$C_{01} = \frac{\gamma_\perp}{\tau_\perp}\frac{1}{\chi_\perp^\infty - \chi_\parallel^0}, \quad C_1 = \frac{\gamma_\parallel}{\left(\chi_\perp^\infty - \chi_\perp^0\right)\tau_\perp}, \quad C_2 = \frac{\gamma_\perp}{\left(\chi_\parallel^\infty - \chi_\perp^0\right)\tau_\parallel},$$
$$C_3 = \left(\frac{\gamma_\parallel}{\tau_\perp} - \frac{\gamma_\perp}{\tau_\parallel}\right)\frac{1}{\chi_\perp^\infty - \chi_\parallel^\infty}, \quad C_4 = \frac{\gamma_\parallel}{\left(\chi_\perp^\infty - \chi_\parallel^0\right)\tau_\perp}.$$

TABLE II. Summary of the conditions to achieve stable states for spheroids.

Stable states	Prolate (bistability)	Oblate (no bistablity)
Nonspinning	$\theta = 0$ $C_{01} < 0$ $C_{01} > 0$, $E_0^2 < C_{01}$	$\theta = \pi/2$ $C_1 < 0$ $C_2 > 0$, $E_0^2 < \min(C_1, C_2)$ $C_1 > 0$, $C_2 < 0$, $E_0^2 < C_1$
Spinning	$\theta = \pi/2$ $C_1 > 0$, $C_3 > C_4 > 0$, $C_3 > E_0^2 > C_4$	$\theta = \pi/2$ $C_1 > 0$, $E_0^2 > \max(C_1, C_3)$

For a thin disk $\gamma_\parallel = \gamma_\perp$, the parameters C_1, C_2, and C_3 can be simplified using Eqs. (2)–(4),

$$C_1 = \frac{\gamma_\parallel}{(\chi_\perp^\infty - \chi_\perp^0)\tau_\perp} = \frac{C_0}{\varepsilon_p/\varepsilon_f - \sigma_p/\sigma_f}, \quad C_0 = \frac{\gamma_\parallel}{\tau_\perp \varepsilon_f}, \tag{B18}$$

$$C_2 = \frac{\gamma_\perp}{(\chi_\parallel^\infty - \chi_\perp^0)\tau_\parallel} = \frac{\varepsilon_f}{\varepsilon_p}\frac{\sigma_p}{\sigma_f}\frac{C_0}{2 - \sigma_p/\sigma_f - \varepsilon_f/\varepsilon_p}, \tag{B19}$$

$$C_3 = \left(\frac{\gamma_\parallel}{\tau_\perp} - \frac{\gamma_\perp}{\tau_\parallel}\right)\frac{1}{\chi_\perp^\infty - \chi_\parallel^\infty} = \left(1 - \frac{\varepsilon_f}{\sigma_f}\frac{\sigma_p}{\varepsilon_p}\right)\frac{C_0}{\varepsilon_p/\varepsilon_f + \varepsilon_f/\varepsilon_p - 2}, \tag{B20}$$

which are equivalent to Eqs. (11), (12), and (15).

[1] G. Quincke, Ueber rotationen im constanten electrischen felde, Ann. Phys. (Leipzig) **295**, 417 (1896).
[2] T. B. Jones, Quincke rotation of spheres, IEEE Trans. Ind. Appl. **20**, 845 (1984).
[3] T. B. Jones, *Electromechanics of Particles* (Cambridge University Press, Cambridge, 2005).
[4] L. Lobry and E. Lemaire, Viscosity decrease induced by a DC electric field in a suspension, J Electrostat. **47**, 61 (1999).
[5] A. Cēbers, Bistability and "Negative" Viscosity for a Suspension of Insulating Particles in an Electric Field, Phys. Rev. Lett. **92**, 034501 (2004).
[6] N. Pannacci, E. Lemaire, and L. Lobry, DC conductivity of a suspension of insulating particles with internal rotation, Eur. Phys. J. E **28**, 411 (2009).
[7] A. O. Tseber, Certain peculiarities of transport phenomena in suspensions with internal rotations, J. Appl. Math. Mech. **42**, 716 (1978).
[8] P. F. Salipante and P. M. Vlahovska, Electrohydrodynamics of drops in strong uniform dc electric fields, Phys. Fluids **22**, 112110 (2010).
[9] O. D. Lavrentovich, Transport of particles in liquid crystals, Soft Matter **10**, 1264 (2014).
[10] K. Yeo, E. Lushi, and P. M. Vlahovska, Collective Dynamics in a Binary Mixture of Hydrodynamically Coupled Microrotors, Phys. Rev. Lett. **114**, 188301 (2015).
[11] M. Belovs and A. Cēbers, Relaxation of polar order in suspensions with Quincke effect, Phys. Rev. E **89**, 052310 (2014).
[12] R. H. Bube, *Photoconductivity of Solids* (Krieger, Huntington, 1978).
[13] Q. Brosseau, G. Hickey, and P. M. Vlahovska, Electrohydrodynamic Quincke rotation of a prolate ellipsoid, Phys. Rev. Fluids **2**, 014101 (2017).
[14] A. Cēbers, E. Lemaire, and L. Lobry, Electrohydrodynamic instabilities and orientation of dielectric ellipsoids in low-conducting fluids, Phys. Rev. E **63**, 016301 (2001).

[15] Y. Dolinsky and T. Elperin, Dipole interaction of the Quincke rotating particles, Phys. Rev. E **85**, 026608 (2012).
[16] M. Antal, G. Filipcsei, and M. Zrinyi, Direct observation of Quincke rotation of disk shaped polymer composites in a uniform DC electric field, Compos. Sci. Technol. **67**, 2884 (2007).
[17] R. A. Bauer, L. Kelemen, M. Nakano, A. Totsuka, and M. Zrinyi, Fabrication and electrorotation of a novel epoxy based micromotor working in a uniform DC electric field, Smart Mater. Struct. **24**, 105010 (2015).
[18] Y. Gu and K. G. Kornev, Ferromagnetic nanorods in applications to control of the in-plane anisotropy of composite films and for in situ characterization of the film rheology, Adv Funct Mater **26**, 3796 (2016).
[19] A. Tokarev, A. Aprelev, M. N. Zakharov, G. Korneva, Y. Gogotsi, and K. G. Kornev, Multifunctional magnetic rotator for micro and nanorheological studies, Rev. Sci. Instrum. **83**, 065110 (2012).
[20] Y. Gu, Z. X. Chen, N. Borodinov, I. Luzinov, F. Peng, and K. G. Kornev, Kinetics of evaporation and gel formation in thin films of ceramic precursors, Langmuir **30**, 14638 (2014).
[21] K. G. Kornev, Y. Gu, P. Aprelev, and A. Tokarev, in *Magnetic Characterization Techniques for Nanomaterials* (Springer, Berlin, 2017), p. 51.
[22] A. O. Tsebers, Internal rotation in the hydrodynamics of weakly conducting dielectric suspensions, Fluid Dyn. **15**, 245 (1980).
[23] A. O. Tsebers, Electrohydrodynamic instabilities in a weakly conducting suspension of ellipsoidal particles, Magnetohydrodynamics **16**, 175 (1980).
[24] S. H. Strogatz, *Nonlinear Dynamics and Chaos: With Applications to Physics, Biology, Chemistry, and Engineering* (Westview, Boulder, 2015).
[25] L. D. Landau and E. M. Lifshitz, *Fluid Mechanics*, Course of Theoretical Physics Vol. 6 (Pergamon Press, Oxford, 1987).
[26] D. B. Dusenbery, *Living at Micro Scale: The Unexpected Physics of Being Small* (Harvard University Press, Cambridge, 2009).